

See discussions, stats, and author profiles for this publication at: <https://www.researchgate.net/publication/257817253>

Calculation of Manoeuvring Forces on Submarines Using Two Viscous-Flow Solvers

Conference Paper · June 2010

DOI: 10.1115/OMAE2010-20373

CITATIONS
36

READS
509

3 authors:



Guilherme Vaz
Maritime Research Institute Netherlands
122 PUBLICATIONS 866 CITATIONS

[SEE PROFILE](#)



Serge Toxopeus
Maritime Research Institute Netherlands
61 PUBLICATIONS 304 CITATIONS

[SEE PROFILE](#)



Samuel Holmes
Red Wing Engineering, Inc.
25 PUBLICATIONS 148 CITATIONS

[SEE PROFILE](#)

Some of the authors of this publication are also working on these related projects:



PROCAL-potential flow code for propellers&cavitation [View project](#)



WWW.refresco.org [View project](#)

CALCULATION OF MANOEUVRING FORCES ON SUBMARINES USING TWO VISCOSUS-FLOW SOLVERS

Guilherme Vaz

MARIN

R&D Department, CFD Projects
P.O. Box 28, 6700 AA Wageningen
The Netherlands
g.vaz@marin.nl

Serge Toxopeus

MARIN / Delft University of Technology
R&D Department, CFD Projects
P.O. Box 28, 6700 AA Wageningen
The Netherlands
s.l.toxopeus@marin.nl

Samuel Holmes

Red Wing Engineering, Inc.
2685 Marine Way, Suite 1421
Mountain View, CA 94043
USA
samuel.holmes@redwingengineering.com

ABSTRACT

Submersibles used for exploration, maintenance and naval warfare have to be both manoeuvrable and easy to control. Simulation of the trajectory for these vessels requires the accurate determination of the hydrodynamic forces and moments which are determined by model-testing, empirical methods or a combination of both. CFD can play a role here by permitting an easier and more accurate determination of these loads. In this paper we focus on the accurate prediction of the manoeuvring forces of free swimming streamlined submersibles (submarines) using CFD. We compare simulations of a standardised well-known submarine shape (DARPA SUBOFF) for two configurations, one bare hull (AFF-1) and one fully-appended hull (AFF-8), under different inflow angles. The viscous-flow solvers used are the finite volume solver ReFRESCO developed by MARIN, and the finite element commercial solver AcuSolve. Verification studies are performed and the numerical results are validated with the experimental data available in the literature. The influence of different turbulence models is investigated and results obtained with a RANS (Reynolds-Averaged-Navier-Stokes) approach are compared with the theoretically more realistic DDES (Delayed-Detached-Eddy-Simulation) results. The influence of the appendages on the forces and flow fields is also investigated and analysed. As a last example, results of a forced pitch motion including dynamic effects are presented.

INTRODUCTION

Both manned and unmanned underwater vehicles are widely used for research, equipment installation and maintenance, and as weapons. The increased sophistication and changes in operational environment of these systems have put a new emphasis on all aspects of design including hydrodynamic performance. The problem of designing submarine vehicles for low drag and good handling and stability has been the subject of many studies dating back to the beginning of the last century. These vehicles need to be both manoeuvrable and easy to control. The simulation of the behaviour of these vessels needs the accurate

determination of the hydrodynamic loads which are usually still determined by model-testing, empirical methods or a combination of both. CFD (Computational Fluid Dynamics) methods can play a role here by permitting an easier and more accurate determination of the forces on the submarines subjected to different flow conditions. CFD tools have been used for this purpose since the beginning of the 1990s, [1], and it is becoming a mature approach where RANS (Reynolds-averaged-Navier-Stokes), DES (Detached-Eddy-Simulation) and even LES (Large-Eddy-simulations) methods are applied (see for instance [2]). CFD is in this case attractive: 1) model-testing for submersibles is difficult, expensive, and requires stingers or struts to support the model; 2) semi-empirical methods sometimes disregard several non-linear effects and are often based on potential flow assumptions; 3) CFD requires few approximations, includes viscous effects, can obtain solutions for full-scale Reynolds numbers and can, if the computational power is available, consider dynamic effects.

Submarine motions are predicted by calculating the forces and moments on the ship and integrating the equations of motions in time. Using state-of-the-art CFD tools one can calculate the forces and moments of the submarine for a range of arbitrary manoeuvring conditions and solve the equations of motions separately, or really simulate the manoeuvre by coupling the equations of motion with the fluid flow equations. While the full time simulation may be too prohibitive for design or analysis purposes, the calculation of the hydrodynamic loads for given conditions is nowadays feasible and is demonstrated in this paper. Nevertheless, as an illustration of what currently can be done with CFD tools for manoeuvres, we will briefly show a test case where dynamic response is calculated directly.

Toxopeus and Vaz [3] previously addressed the flow around the bare-hull DARPA SUBOFF configuration and completed verification and validation exercises. The results showed small numerical errors and good accuracy when compared with the experimental data. Nevertheless, several recommendations for further work were made: finer grids should be considered; the unsteady

behaviour for the larger inflow angles should be investigated; different turbulence models should be checked, and maybe a RANS v.s. DES/LES comparison should be done at large angles; a more realistic submarine should be additionally considered. In the current paper we tackle these issues. Further computations on the AFF-1 configuration are presented for small and large inflow angles and for finer grids. A new technique for speeding-up the computation of the forces and moments for a range of inflow angles is also presented. For angles above 18° there are no experimental data. Therefore, we compare the results obtained using two completely different codes, MARIN *ReFRESCO* and the commercial code *AcuSolve*. Forces obtained with a RANS and a theoretically more accurate DES approach are compared. For an appended submarine hull form (AFF-8), *ReFRESCO* computations are performed for two inflow angles and the forces, flow fields and propeller plane wake-fields studied. Using *AcuSolve*, results of a computation for a forced-pitching manoeuvre are presented.

The paper is organised as follows: after this introduction, the setup of all computations and codes is explained, together with the geometry and grids used. After that, the AFF-1 results are shown and analysed, followed by the AFF-8 configuration. Finally, conclusions and recommendations are drawn.

NUMERICAL SETUP

Geometry

The DARPA SUBOFF submarine hull form [4,5,6] has been selected as test case because of the availability of extensive validation data for flow field variables and integral quantities. In literature, several other studies concerning calculations on the bare-hull DARPA SUBOFF (designated configuration AFF-1 as defined in Liu and Huang [6]) can be found, see e.g. Sung et al. [1], Bull [7], and Yang and Löhner [8]. For the appended DARPA SUBOFF case (designated configuration AFF-8), several CFD studies have been also published, see e.g. Alin et al. [9] or Huuva [2].

The main particulars of the DARPA SUBOFF are specified in Table 1 and shown in Figure 1.

Table 1. Main particulars of DARPA SUBOFF submarine

Description	Symbol	Magnitude	Unit
Length overall	L_{oa}	4.356	m
Length between perpendiculars	L_{pp}	4.261	m
Maximum hull radius	R_{\max}	0.254	m
Centre of buoyancy (aft of nose)	FB	0.4621 L_{oa}	-
Volume of displacement (AFF-1)	∇	0.708	m^3
Wetted surface (AFF-1)	S_{wa}	5.998	m^2
Volume of displacement (AFF-8)	∇	0.718	m^3
Wetted surface (AFF-8)	S_{wa}	6.338	m^2

Definitions

The same definitions as used during the experiments were adopted, to allow easy comparison with other results published in literature. The origin of the right-handed system of axes used in this study is located at the intersection of the longitudinal axis of symmetry of the hull and the forward perpendicular plane, with x directed aft, y to starboard and z vertically upward. All coordinates given in this paper are made non-dimensional with the

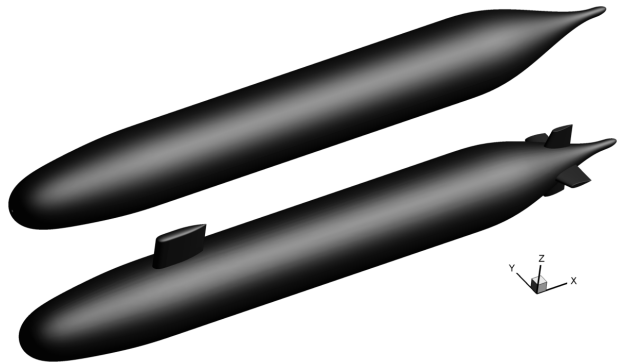


Figure 1. DARPA SUBOFF Geometry (Top: AFF-1 Configuration. Bottom: AFF-8 Configuration)

overall length L_{oa} of the submarine ($L_{\text{oa}} = 4.356\text{m}$). The velocity field $\mathbf{V} = (u, v, w)$ is made non-dimensional with the undisturbed velocity V_0 . The drift or inflow angle is defined by $\beta = \arctan \frac{v}{u}$, with u and v directed according to the x and y axes respectively, which means that β is positive for flow coming from port side.

All integral forces and moments on the hull are based on a right-handed system of axes corresponding to positive directions normally applied in manoeuvring studies. This means that the X force is directed forward, Y to starboard and Z vertically down. Similar to the results presented by Roddy [10], all moments are given with respect to the centre of gravity, which is located at $0.4621L_{\text{oa}}$ aft of the nose of the model. Non-dimensionalisation is done with the length between perpendiculars ($L_{\text{pp}} = 4.261\text{m}$) using $X, Y, Z / \frac{1}{2}\rho V_0^2 L_{\text{pp}}^2$ and $K, M, N / \frac{1}{2}\rho V_0^2 L_{\text{pp}}^3$. The pressure coefficient C_p is defined as $C_p = (p - p_0) / \frac{1}{2}\rho V_0^2$, p_0 being the undisturbed pressure, and the skin friction coefficient C_f as $C_f = |\vec{\tau}| / \frac{1}{2}\rho V_0^2$. A reference time $t_0 = L_{\text{pp}} / V_0$ is also considered.

Solvers

ReFRESCO is a MARIN spin-off of *FreSCo* [11], which was developed within the VIRTUE EU Project together with TUHH and HSVA. *ReFRESCO* is an acronym for *Reliable & Fast Rans Equations (solver for) Ships, Cavitation & Offshore*. It solves the multi-phase unsteady incompressible RANS (Reynolds-averaged Navier-Stokes) equations, complemented with turbulence models and volume-fraction transport equations for each phase. The equations are discretised using a finite-volume approach with cell-centred collocated variables. The implementation is face-based, which permits grids with elements with an arbitrary number of faces (hexahedrals, tetrahedrals, prisms, pyramids, etc.). The code is parallelised using MPI and sub-domain decomposition. Low order and higher-order spatial and temporal discretisation schemes are available in the code. The equations are solved in a segregated approach, and the pressure/velocity coupling is solved using the SIMPLE algorithm. The code is targeted, optimised and highly validated for hydrodynamic applications, in particular for current, wind and manoeuvring coefficients of ships, submersibles and semi-submersibles, see [12, 3, 13, 14].

AcuSolve is a finite-element commercial CFD solver from ACUSIM Software. *AcuSolve* is based on the Galerkin/Least-Squares (GLS) formulation [15, 16]. The GLS formulation provides second order accuracy for spatial discretisation of all variables. In addition to satisfying conservation laws globally, the formulation ensures local conservation for individual elements.

Equal-order nodal interpolation is used for all working variables, including pressure and turbulence equations. The semi-discrete generalised-alpha method [17] is used to integrate the equations in time for transient simulations. The resultant system of equations is solved as a fully coupled pressure/velocity matrix system using a preconditioned iterative linear solver. Previous applications with *AcuSolve* and DES for offshore blunt-body type of flows can be seen in [18, 19].

Domain and Boundary Conditions

The computational domains and boundary conditions used differ for the two geometries and the two codes. Figure 2 shows the settings used for *ReFRESCO*. For the steady computations, the symmetry of the flow was taken into account and a half-sphere domain is used together with a no-slip boundary condition (b.c.) on the hull, a symmetry b.c. on the symmetry plane, and a so-called *AutoDetect* b.c. This last boundary condition detects automatically, depending on the direction of the incoming flow \mathbf{V}_0 , which boundary faces are Inflow-type faces and which ones are Outflow-type. This permits to study a complete range of inflow angles with no changes to the grid layout. When unsteady computations are performed, no symmetry plane can be used otherwise no vortex-shedding occurs. Therefore, the computational domain is vertically mirrored in order to obtain a complete sphere. For the AFF-8 case a more usual domain configuration is used as can be seen in Figure 2. For the side, bottom and top walls a so-called *Pressure* b.c. is used to minimise blockage effects: the pressure is fixed to the reference pressure p_0 and a zero normal velocity gradient b.c. is enforced.

The computational domain used for all *AcuSolve* computations is illustrated in Figure 3. It is similar to the one in Figure 2, except that a free-slip b.c. is used on the lateral walls. In order to facilitate the simulation of different inflow angles, the domain is divided into two parts: one fixed sub-domain and one rotating sub-domain. The inner sub-domain around the submarine is rotated around the z axis in order to change the orientation of the flow with respect to the submarine. A fluid-fluid interface, illustrated in green in Figure 3, is used to connect the fixed and the rotating sub-domains so that large rotations can be handled dynamically without mesh distortion.

Grids

For the computations done with *ReFRESCO*, the grids used are fully (block) structured O-O grids with finer resolution close to all No-Slip walls, in this case the submarine hull and appendages. No wall functions are used and for all computations the non-dimensional wall distance y_2^+ is smaller than 1. For AFF-1 the grids were generated using an in-house structured multi-block grid generator. For AFF-8 the commercial grid generation package *GridPro* was used. Figure 4 show the grid on the hull of AFF-8, a slice for the $y = 0$ plane, and some details close to the bow and the stern of the vessel. The grids done with *GridPro*, even for the AFF-8 more complex geometry, present high smoothness and orthogonality to the boundaries, characteristics that help the iterative convergence but also the accuracy of the solution. Details on the grids used (on total 11 for the AFF-1 and 4 for the AFF-8) are given in Table 2 and Table 4.

For *AcuSolve* two unstructured meshes were generated directly from a CAD description of the hulls using the automatic mesh generator *AcuConsole*. An overall view of the coarse mesh

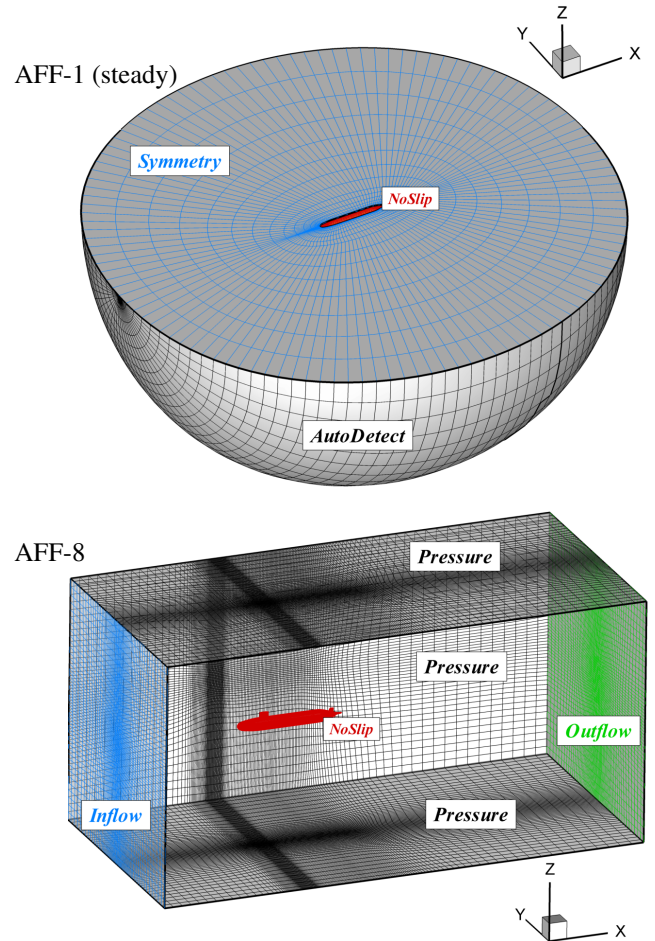


Figure 2. *ReFRESCO* domain and boundary conditions

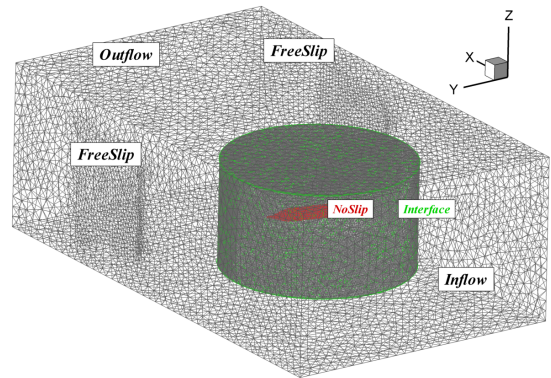


Figure 3. *AcuSolve* domain and Boundary Conditions

is shown in Figure 5. The coarse mesh contains 2.1M nodes with 527K wedge elements in the boundary layer (in red in Figure 5). The first element thickness is chosen to give an average y_2^+ of about 30. The maximum y_2^+ ever observed in any of the calculations was 70. The fine mesh contains 4.4M nodes with 1.76M wedge elements in the boundary layer.

Solver Settings

The computations done by *ReFRESCO* are rather steady or unsteady RANS, using the one-equation Spalart&Allmaras (SA) [20] or Menter's SST version [21] of the two-equation $k - \omega$ turbulence models. For the convection scheme of the momentum equations a QUICK 2nd – 3rd order scheme and for the turbulence equations an 1st order upwind scheme is used. For all

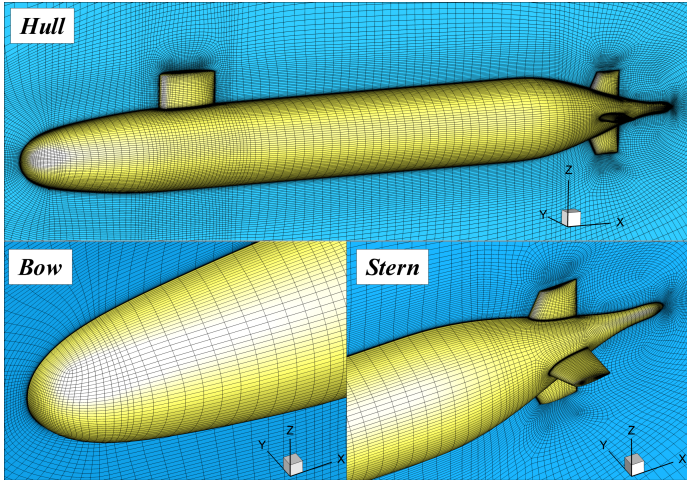


Figure 4. *ReFresco* Grid-4 for AFF-8 configuration

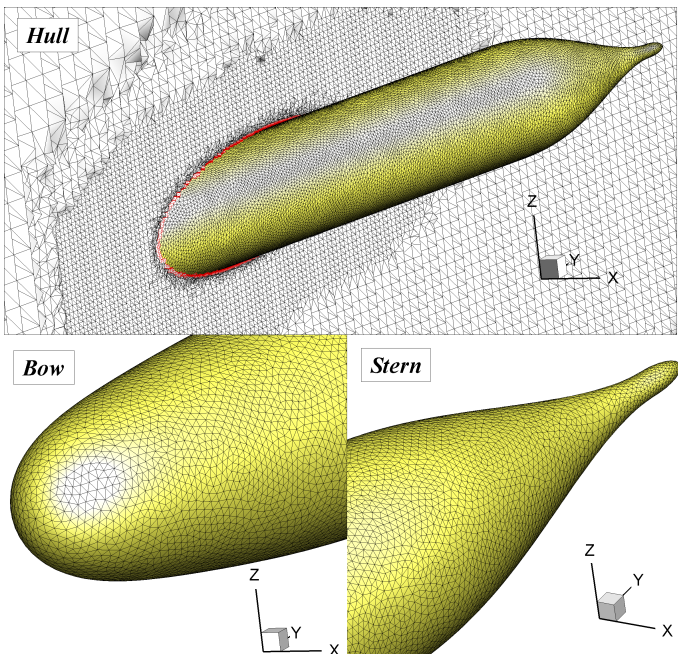


Figure 5. *AcuSolve* Grid-2 for AFF-1 configuration, $\beta = 75^\circ$

diffusion terms a 2nd order central discretisation scheme is considered. For unsteady computations a 2nd order three-time-level scheme is used. The effect of the time discretisation step, Δt , is briefly studied. No wall functions are needed. All computations use as initial condition an undisturbed flow field and constant pressure field.

The computations done by *AcuSolve* use Spalart's *Delayed Detached Eddy Simulation* (DDES) model to capture turbulence effects [22]. The model treats the flow as a Reynolds Averaged Navier-Stokes (RANS) calculation in the boundary layer and as a Large Eddy Simulation (LES) elsewhere. It is thus more economical than a true LES simulation which requires a finer mesh in the boundary layer. The one-equation Spalart&Allmaras (SA) [20] is the basis for the RANS formulation in the DDES turbulence model. This model is an improved version of the usual DES (*Detached Eddy Simulation*), which is characterised by less grid-dependency with respect to the RANS-LES transition zone, a typical issue of the original DES model. All computations were done in unsteady mode with a time step of $\Delta t = t_0/15.75 = 0.1s$

Table 2. *ReFresco* calculations for SUBOFF AFF-1 configuration

Grid	Total,Hull [k]Cells	TurbModel	Angle [°]	$\Delta t/t_0$	$Re \times 10^{-6}$
1	4138, 35.10	SST	0°	No	12, 14
1	4138, 35.10	SST	0-24°	No	14
1	4138, 35.10	SA	0°	No	12, 14
2	2859, 26.88	SST	0°	No	14
3	1626, 17.40	SST	0°	No	14
4	1039, 13.60	SST	0°	No	14
5	538, 8.77	SST	0°	No	14
6	366, 6.72	SST	0°	No	14
6	366, 6.72	SST	0-24°	No	14
7	147, 4.60	SST	0°	No	14
8	134, 3.40	SST	0°	No	14
9	48, 1.68	SST	0°	No	14
1	4138, 35.10	SST	18°	No	14
1	4138, 35.10	SA	18°	No	12, 14
1	4138, 35.10	SST	2°	No	12, 14
1	4138, 35.10	SA	2°	No	12, 14
6	366, 6.72	SST	26°	No	14
6	366, 6.72	SST	36°	No	14
6	366, 6.72	SST	60°	No	14
6	366, 6.72	SST	75°	No	14
6	366, 6.72	SST	90°	No	14
6	366, 6.72	SST	90°	1/20	14
6	2 × 366 , 12.64	SST	90°	1/20	14
6	2 × 366 , 12.64	SST	90°	1/90	14
4	2 × 1039 , 26.88	SST	90°	1/50	12
4	2 × 1039 , 26.88	SST	90°	1/200	12
4	2 × 1039 , 26.88	SST	75°	1/100	12
4	2 × 1039 , 26.88	SST	75°	1/200	12
4	2 × 1039 , 26.88	SA	75°	1/200	12
4	2 × 1039 , 26.88	SST	75°	1/400	12

Table 3. *AcuSolve* calculations for SUBOFF AFF-1 configuration

Grid	Total,Hull [k]Nodes	TurbModel	Angle	$\Delta t/t_0$	$Re \times 10^{-6}$
1	4402, 73.56	SA-DDES	0°	1/15.8	12, 14
2	2089, 21.96	SA-DDES	0°	1/15.8	12, 14
2	2089, 21.96	SA-DDES	2°	1/15.8	14
2	2089, 21.96	SA-DDES	4°	1/15.8	14
2	2089, 21.96	SA-DDES	6°	1/15.8	14
2	2089, 21.96	SA-DDES	10°	1/15.8	14
2	2089, 21.96	SA-DDES	18°	1/15.8	14
2	2089, 21.96	SA-DDES	60°	1/52.5	14
2	2089, 21.96	SA-DDES	75°	1/52.5	14

Table 4. *ReFresco* calculations for SUBOFF AFF-8 configuration

Grid	Total,Hull [k]Cells	TurbModel	Angle	Unstd.	$Re \times 10^{-6}$
1	4866, 68.00	SST	0°	No	12
2	2475, 36.76	SST	0°	No	12
3	1191, 22.73	SST	0°	No	12
3	2 × 1191, 45.46	SST	0°	No	12
3	2 × 1191, 45.46	SST	18°	No	12

(for low angles) or $\Delta t = t_0/52.5 = 0.03s$ (for larger angles).

Summary of Computations Performed

Calculations for inflow angles ranging from 0° up to 90° were conducted for the AFF-1 configuration. For the AFF-8 configuration only 0° and 18° have been calculated. Both individual computations for discrete angles and computations with sweeping through a range of angles have been performed (see below). With *ReFresco* several grids have been used for the straight flight (0°) condition in order to study the spatial discretisation error. The temporal discretisation error has been studied for the large angles. All calculations were conducted for deeply submerged condition, so that free surface effects are absent. Based on reference inflow velocities V_0 on model scale of 2.7658 and 3.2268 m/s, and on L_{oa} , the Reynolds numbers Re corresponded to respectively 12×10^6 (used for 0° and 2° for AFF-1 and for AFF-8) and 14×10^6 (used for all drift angles for AFF-1). The set of computations done is shown in Tables 2 through 4.

"One-Computation" Approach

The *ReFresco* calculations for $Re = 14 \times 10^6$ have been

conducted using the finest grid in one computation with an automated procedure. The computation was started from a drift angle of $\beta = 0^\circ$ and after a predefined number of iterations, the inflow angle was changed by 2° . Due to the use of the *AutoDetect* boundary conditions, the inflow and outflow faces are automatically detected and this will allow the flow to cross the computational domain according to the specified new inflow direction. This procedure was repeated until the $\beta = 24^\circ$ drift angle was completed. Using this approach, an improvement of the computational performance of *ReFRESCO* is achieved, while simplifying the administrative tasks the user has to conduct to obtain all drift angle results.

RESULTS FOR AFF-1 CONFIGURATION

Iterative Error

In Figure 6, the iterative convergence history for the straight-ahead sailing condition and the finest grid is presented for *ReFRESCO*. All results are given in non-dimensional values. It is seen that after some initial transients, the L_∞ norms of the pressure, velocity and turbulence components converge smoothly to below $5 \cdot 10^{-6}$. The convergence for *AcuSolve* for the coarse grid is given in Figure 7. In *AcuSolve*, a static solution is usually declared acceptable if the pressure and velocity residuals are below 1×10^{-3} .

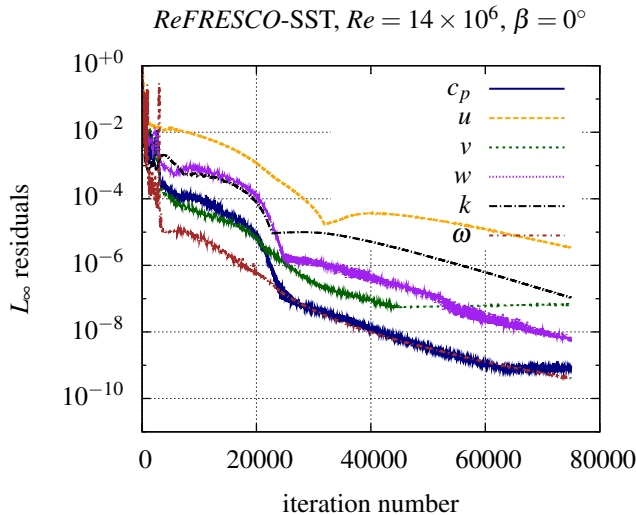


Figure 6. Convergence history of local quantities, *ReFRESCO*-SST

In Figure 8, the iterative convergence history of the transverse force for the calculation in which the drift angle was progressively increased from $\beta = 0^\circ$ to $\beta = 24^\circ$ is presented. These results are given as the change in non-dimensional values. It is seen that at the end of each drift angle, the changes in the transverse force are around or less than 10^{-10} , which indicates iterative convergence. The convergence of the other force or moment coefficients is similar. Based on these aforementioned observations and the fact that other calculations show similar convergence histories, iterative convergence errors in the calculations are assumed to be negligible with respect to discretisation or modelling errors.

Discretisation Error

In order to determine and demonstrate the accuracy and reliability of solutions of viscous flow calculations, grid dependency

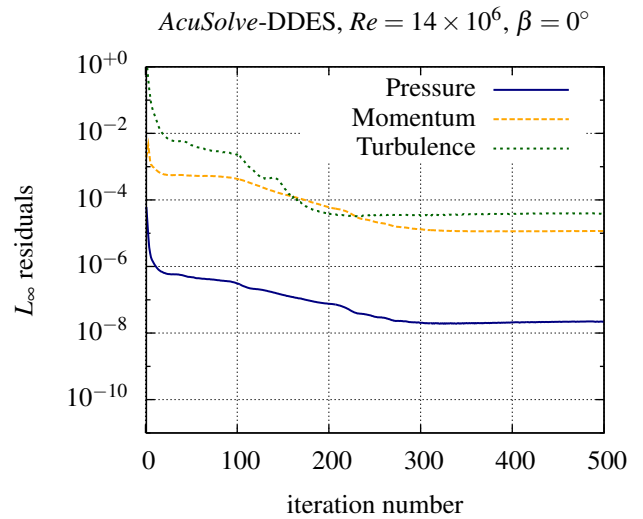


Figure 7. Convergence history of local quantities, *AcuSolve*-DDES

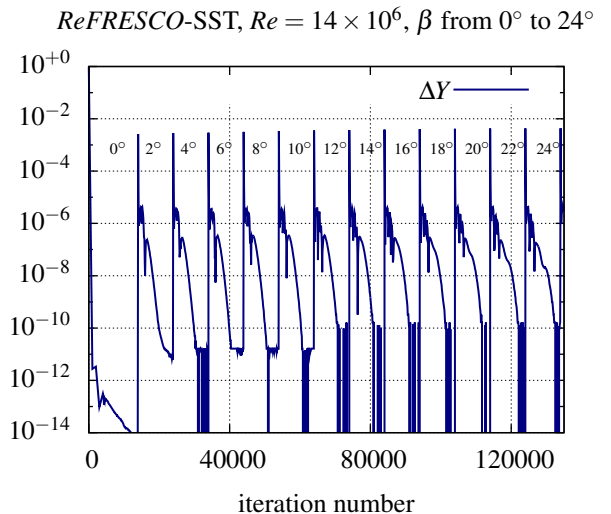


Figure 8. Convergence history of integral quantities, *ReFRESCO*-SST

studies are very important. Several methods for uncertainty analysis are available in literature. In the present work, the method proposed by Eça and Hoekstra [23] is followed.

For $Re = 14 \times 10^6$, the discretisation error in the *ReFRESCO* results for $\beta = 0^\circ$ has been investigated, see Table 5 and Figure 9. The relative step-size h_i/h_1 indicates the coarseness of the grid with respect to the finest grid h_1 . The value of the solution obtained at the finest grid is indicated by ϕ_1 , while ϕ_0 is an estimate of the solution for zero cell size. The graphs show that scatter exists in the data: the data points are not exactly aligned according to the curve. Reasons for this might be e.g. the non-evenly spaced cell nodes, the use of numerical limiters or lack of perfect geometrical similarity between the grids. For this high Reynolds number, i.e. when convection dominates, and when using an unstructured-grid QUICK scheme for convective fluxes, it is expected that *ReFRESCO* will be second order accurate. The observed order of convergence p depends on the force component under consideration. For the friction force, a value just below 1 is found, indicating that the convergence with grid refinement follows a linear order of accuracy. For the other components, a much higher order is found, which most probably is

caused by scatter and insufficiently fine grids. In the previous study by Toxopeus and Vaz [3], the convergence appeared to be better. However, comparing the old (*FreSCO*) results with the new (*ReFRESCO*) results with a finer grid added, it is seen that now the four finest grids show a more consistent trend than the four finest grids in the previous study. The present results are therefore judged to be more reliable. The overall uncertainty U in X is 2.8% which is judged to be small.

An uncertainty study for *AcuSolve* was outside of the scope of work for this paper, since for DES/DDES/LES or DNS calculations this is not a trivial task.

Table 5. Uncertainty analysis, $X, \beta = 0^\circ$

Item	ϕ_0	ϕ_1	U_ϕ	p
X	-1.11×10^{-3}	-1.10×10^{-3}	2.8%	5.05
X_p	-1.22×10^{-4}	-1.29×10^{-4}	19.0%	6.71
X_f	-1.00×10^{-3}	-9.67×10^{-4}	4.4%	0.97

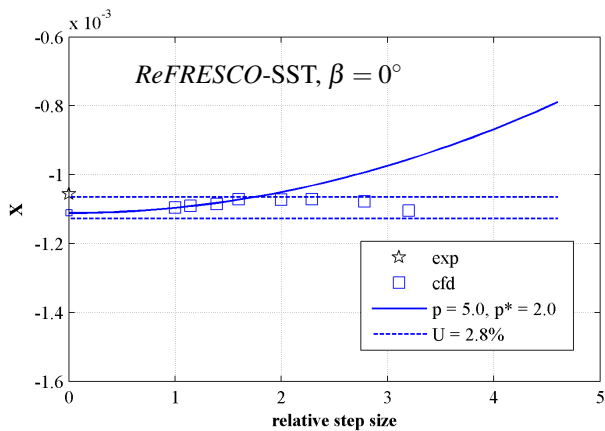


Figure 9. Discretisation uncertainty analysis

Validation

Integral values, straight flight Experimental force measurement results are available for the straight-ahead condition and were published by Roddy [10]. The experiments were conducted in the towing basin of the David Taylor Research Center. During the tests, the model was supported by two struts. The speed used during the experiments resulted in a Reynolds number of 14×10^6 . For this condition the experimental value of the longitudinal force was found to be:

$$X = \text{average}(X_{\text{test1}}, X_{\text{test2}}) = -1.056 \times 10^{-3}.$$

A detailed uncertainty analysis of the force measurements was not conducted. However, to obtain an estimate of the uncertainty in the experimental data, the uncertainty U_D in the experimental data is estimated using a factor of safety of 1.25 by

$$U_D = 1.25 \times \text{abs}(X_{\text{test1}} - X_{\text{test2}}) = 1.25 \times 10^{-5} = 1.2\% \times X.$$

Table 6 presents the longitudinal force components obtained from the calculations. As can be expected for submarine hull forms, the largest part (about 90%) of the total resistance is caused by friction resistance. This means that for the bare hull, the form factor is relatively low, i.e. $(1+k) = X/X_f = 1.13$ for *ReFRESCO-SST* and 1.07 for *ReFRESCO-SA*. For the experiments, the form factor is estimated to be $(1+k) = X/X_f(\text{ITTC}) = 1.13$. This is a normal value for a bare hull submarine.

The difference ε_X between the *ReFRESCO* prediction of X and the measurement is about 3.7% for SST and -3.7% for SA, which are judged to be reasonable for practical applications when also the uncertainty in the experimental data is taken into consideration. The *AcuSolve-DDES* prediction is very close to the uncertainty band around the measurements.

Table 6. Longitudinal force X , $Re = 1.4 \times 10^7$, $\beta = 0^\circ$

Solver	Grid	Integral values $\times 10^3$			
		X	X_f	X_p	ε_X (%)
Exp (DTRC)	-	-1.061	-	-	-
Exp (DTRC)	-	-1.051	-	-	-
Mean μ_{exp}		-1.056	-	-	-
ITTC-57		-	-0.936	-	-
Schoenherr		-	-0.919	-	-
Katsui		-	-0.905	-	-
Grigson		-	-0.932	-	-
ReFRESCO-SST	4138×10^3	-1.096	-0.967	-0.129	3.7
ReFRESCO-SA	4138×10^3	-1.017	-0.950	-0.067	-3.7
AcuSolve-DDES	2089×10^3	-1.070	-	-	1.3

Local quantities, straight flight Further experimental values are obtained from flow field and pressure measurements in a wind tunnel conducted by Huang et al. [5]. These experiments were conducted at a Reynolds number of 12×10^6 . Figure 10 shows comparisons between the calculations and the measurements. These graphs show that the differences in pressure coefficient between the results are negligible. For *ReFRESCO* a very small difference between the SST and SA results was found at the stern, which explains the difference in the longitudinal pressure coefficients X_p . For the skin friction coefficient, it is seen that the *ReFRESCO* results with the SA model are in general slightly closer to the experimental data than the *ReFRESCO-SST* and *AcuSolve* results¹. The differences between the results explain the differences in forces found in Table 6.

The predicted distribution of the pressure coefficient is close to the experiments. The trends in the predicted distribution of the friction coefficient correspond well to the trends found in the experiments. Although some discrepancies at the bow and stern area are found, it is concluded that the prediction of the pressure and skin friction coefficients is good. It is noted that the discrepancies at the bow and stern were also present in all results submitted for a collaborative CFD study within the Submarine Hydrodynamics Working Group (SHWG, see www.shwg.org).

The difference between the *ReFRESCO* and *AcuSolve* results for the streamwise and radial velocities at $x = 0.978L_{\text{oa}}$ in the aft part of the hull is considered to be small, except for the magnitudes of the axial velocities close to the wall when comparing the DDES results with the other results. Comparing the computed results with the experiments, it is observed that the trends in the development of the boundary layer are very well predicted by both solvers, but quantitative discrepancies are seen. Especially the magnitudes of the radial velocities are different. It is seen that in the experiments the radial velocity changes sign between $(r - R_0)/R_{\text{max}} = 2$ and $(r - R_0)/R_{\text{max}} = 0.8$, suggesting

¹It should be noted that in interpreting the *AcuSolve* solutions skin friction had to be estimated from the wall function equations because the flow solution is based on the total traction at the surface and does not explicitly provide the tangential components of stresses.

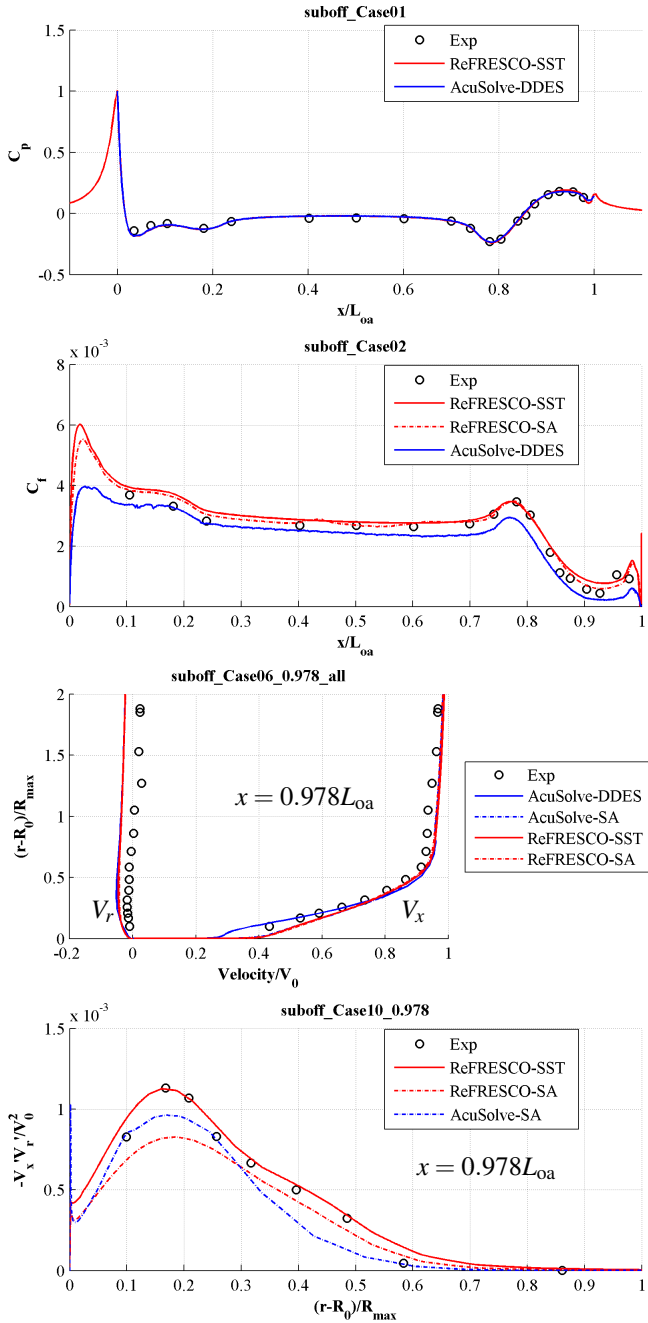


Figure 10. Pressure (top) and skin friction (top-middle) coefficients along the hull, axial and radial velocities (bottom-middle) and Reynolds shear stress (bottom), $\beta = 0^\circ$

outward radial flow in the far field. This may be caused by the use of an open-jet wind tunnel.

Reynolds shear stresses, straight flight In this study, also the correlation between the measured and the predicted Reynolds shear stresses is investigated by comparison of $-\frac{\bar{V}_x'V_r'}{V_0^2}$. Following the eddy-viscosity assumption, the Reynolds

stresses are defined by $-\bar{V}_i'V_j' = 2 \cdot v_t \cdot S_{ij}$, v_t being the eddy viscosity and S_{ij} the strain rate tensor. In Figure 10, the Reynolds shear stresses for $x = 0.978L_{0a}$ are presented. It is observed that curve representing the ReFRESCO-SST results corresponds very well with the measurements. The results using the SA turbulence model are also close to the measurements, but under-predict the peak of the distribution.

Integral quantities, all angles Experimental results for oblique angles were published by Roddy [10]. The experiments were conducted at a Reynolds number Re of 14×10^6 . Figure 11 presents the force and moment components obtained from the calculations and the values from the experiments for oblique inflow.

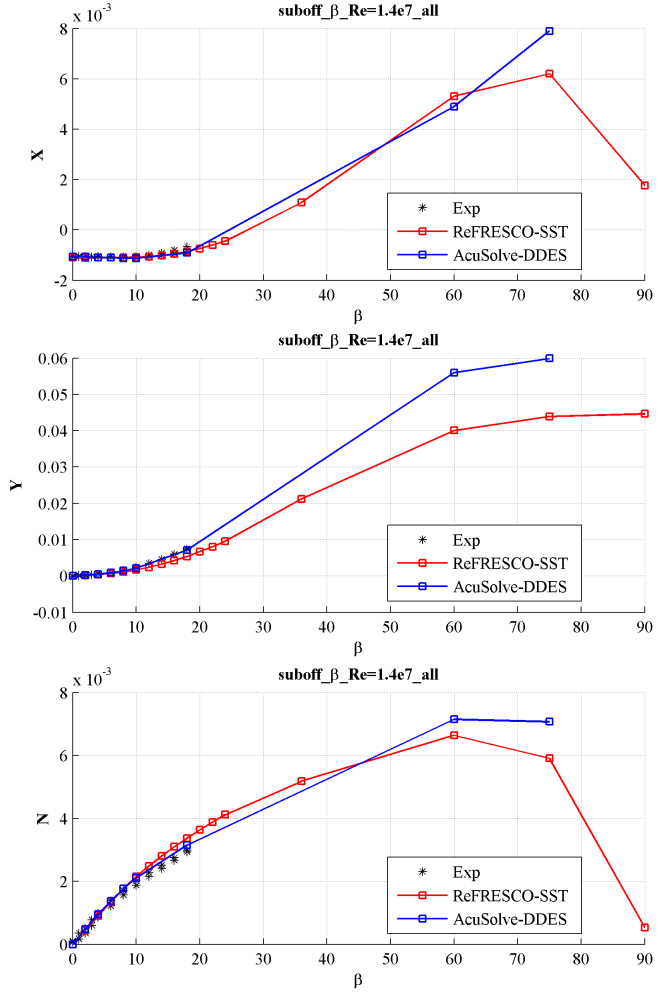


Figure 11. Force and moment coefficients against drift angle

In Tables 7 through 9 the results for $\beta = 18^\circ$ are shown. The deviation ε_X from the measurement is about 13%, which is within the uncertainty band of the measurements. With the SA turbulence model, better agreement is found. The trends in the transverse force Y and yaw moment N are predicted reasonably well, but the AcuSolve results for Y and N are much closer to the measurements. This may be due to the modelling error of using a steady RANS approach, which with increasing inflow angle may be disputable, and less accurate than using a DDES approach. Nevertheless, one should notice that for the AcuSolve results the geometrical blockage is also increasing with the inflow angle. This, together with a free-slip b.c. usually increases the values of the forces. This should be further investigated.

Unsteady effects

In Figure 11, one can see that the differences between a steady RANS approach and an unsteady DDES approach grow with the inflow angle. There are no experiments for this test case for angles larger than 18° . There may exist blockage effects in the AcuSolve results, but the DDES results are expected

Table 7. Longitudinal force X , $Re = 1.4 \times 10^7$, $\beta = 18^\circ$

Solver	Grid	Integral values $\times 10^3$			
		X	X_f	X_p	ε_X (%)
Exp (DTRC)	-	-0.670	-	-	-
Exp (DTRC)	-	-0.852	-	-	-
Mean μ_{exp}		-0.761	-	-	-
ReFRESCO-SST	4138×10^3	-0.860	-1.067	0.207	13.0
ReFRESCO-SA	4138×10^3	-0.767	-1.074	0.307	0.8
AcuSolve-DDES	2089×10^3	-0.910	-	-	19.6

Table 8. Transverse force Y , $Re = 1.4 \times 10^7$, $\beta = 18^\circ$

Solver	Grid	Integral values $\times 10^3$			
		Y	Y_f	Y_p	ε_Y (%)
Exp (DTRC)	-	7.355	-	-	-
Exp (DTRC)	-	7.438	-	-	-
Mean μ_{exp}		7.397	-	-	-
ReFRESCO-SST	4138×10^3	5.383	0.297	5.086	-27.2
ReFRESCO-SA	4138×10^3	5.678	0.307	5.371	-23.2
AcuSolve-DDES	2089×10^3	7.160	-	-	-3.2

Table 9. Yawing moment N , $Re = 1.4 \times 10^7$, $\beta = 18^\circ$

Solver	Grid	Integral values $\times 10^3$			
		N	N_f	N_p	ε_N (%)
Exp (DTRC)	-	2.986	-	-	-
Exp (DTRC)	-	2.939	-	-	-
Mean μ_{exp}		2.962	-	-	-
ReFRESCO-SST	4138×10^3	3.370	0.017	3.353	13.8
ReFRESCO-SA	4138×10^3	3.383	0.017	3.366	14.2
AcuSolve-DDES	2089×10^3	3.150	-	-	6.3

to be more accurate for these cases, since the flow for a bare cylindrical hull and large angles is a blunt-body type of flow (see Figure 21 below). In this case it is known that a steady RANS approach is not valid, and even an unsteady RANS calculation does not simulate correctly the flow for some Reynolds numbers (see for instance [24]). For the large Reynolds numbers here simulated (even based on the hull diameter) *accurate* unsteady RANS simulations are expected to produce reasonable results. However several aspects have to be considered in order to produce *accurate* unsteady RANS results:

- The complete submarine has to be computed, or no vortex shedding occurs.
- The computations have to be unsteady and enough time should be allowed for the vortex shedding to occur. The Von Karman vortex shedding is a flow instability that takes time, both in the reality and in the simulations, to be triggered.
- The time-step has to be fine and has usually a large influence in the results. A coarse time-step and a fine grid can produce wrong results (see [12]).
- The grids have to be fine in all shear layers, and not only on the hull and in the boundary-layers. For this purpose, the structured grids here used are not suitable.

The effect of the unsteadiness and time-step for one grid, an angle of 75° and for the Y coefficient, is shown in Figure 12. The signal is multi-frequency and the averaged values are different than for a steady computation. However, the signal is still not cyclic (as it has to be), and larger simulation times should be considered. This is currently under investigation.

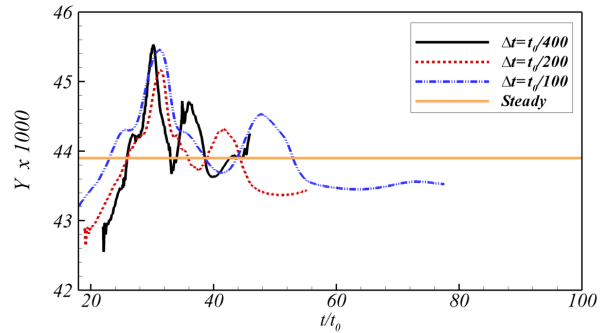


Figure 12. Time history of forces and moments, $ReFRESCO$, $\beta = 75^\circ$

RESULTS FOR AFF-8 CONFIGURATION

Iterative and Discretisation Error

The AFF-8 configuration represents the SUBOFF hull with a sail on the top of the hull and with four wing-type of stern appendages just before the propeller location (which is not considered). The flow around the submarine is therefore more complex, even for straight flight. *GridPro* grids were used for this case. The high quality of these grids is then visible in the good convergence properties and in the iterative and spatial discretisation errors. Figure 13 and Figure 14 show the iterative convergence for the finest grid. The solution is converged to below 3×10^{-6} in both the residuals and the maximum changes of all quantities, within 4000 iterations. For this calculation, some modifications to the input files were made, such as changes in the relaxation parameters and solvers used. Compared with the more simple geometry and flow for AFF-1 and using in-house grids (see Figure 6), this is a large improvement in terms of convergence properties and CPU time needed. The flow solution is steady and the force and moment coefficients do not vary much anymore after 2000 iterations. The iterative error is considered then to be small and does not have influence on the solution nor on the discretisation error.

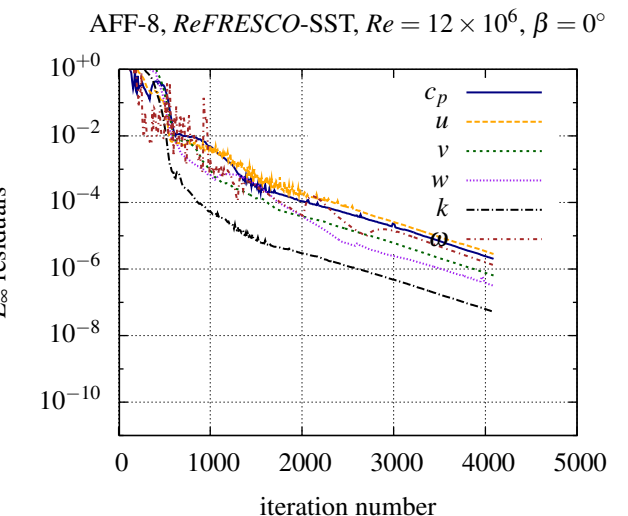


Figure 13. Convergence history of local quantities

In Table 10 one can see the variation of the forces and moments with the grid refinement. Grid-3 (ps/sb) is the same as Grid-3 but considering the complete submarine. Notice that three grids are not enough to perform a reliable verification study, and

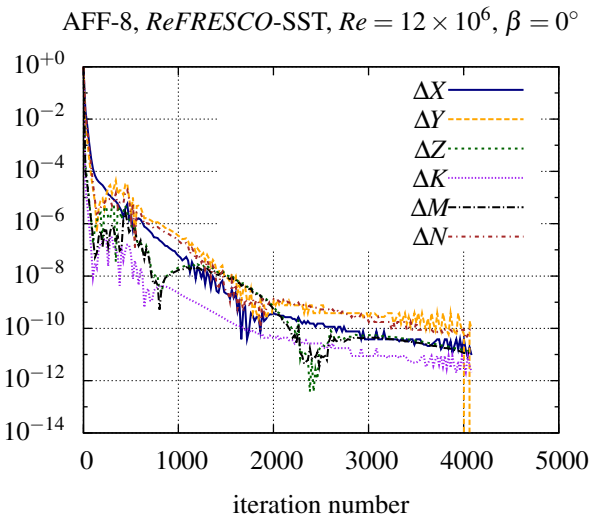


Figure 14. Forces and moments iterative convergence

therefore we are presenting the tabular data without uncertainty estimates. This will be considered in the future. The differences in the largest force, in this case the X drag force, between the results for all grids, are smaller than 1%. There is however some scatter (in the third digit) in the results. The Z and the M moment show a convergence tendency and do not present scatter. With the complete domain the K and the N moments, which should be zero, are indeed negligible.

Grid	X	Y	Z	K	M	N
1	-1.257	0.0	0.007	0.0	0.018	0.0
2	-1.250	0.0	0.008	0.0	0.019	0.0
3	-1.254	0.0	0.010	0.0	0.021	0.0
3 (ps/sb)	-1.263	7.41×10^{-4}	0.011	3.08×10^{-5}	0.022	7.12×10^{-5}
AFF-1 (1)	-1.126	0.0	0.0	0.0	0.0	0.0

For the so-called wake-field at the location of the propeller, $x/L_{pp} = 1.0$ or $x/L_{oa} = 0.978$, Figure 15 shows that the effect of the grid refinement is minimal, the differences being most visible in the wakes of the appendages (sail and stern-wings).

Both the iterative and the grid convergence results here

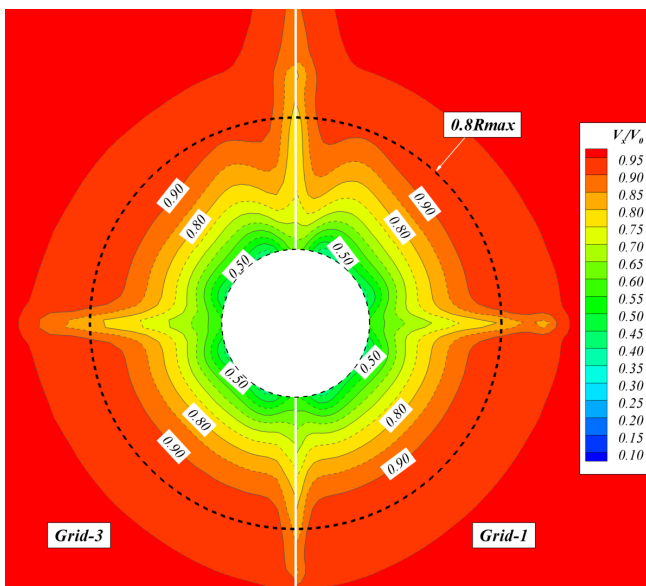


Figure 15. Wake-field V_x/V_0 at $x/L_{oa} = 0.978$, $\beta = 0^\circ$

shown give some confidence that the numerical errors, iterative and discretisation errors, are under control, and do not play a role in the results presented below.

Validation

For the AFF-8 configuration less experimental data is available than for the AFF-1. In Figure 16 one can see a comparison between the numerical results and the experimental data [5] for the C_p distribution along the hull. The agreement is considered good, the experimental data having however low lengthwise resolution. The peaks on the curve coincide with the stagnation points on respectively the bow, the sail and the rudder. Additionally, the wake-field can be also validated with experiments (done unfortunately without the sail). Figure 17 shows the comparison between numerical and experimental results. The effect of absence of the sail in the experiments is seen in the top part of the propeller disk, but for the rest of the field the agreement is considered good. Notice that in the experiments the data was cut off for $r/R_{max} > 0.90$, which is not the case in the CFD calculations.

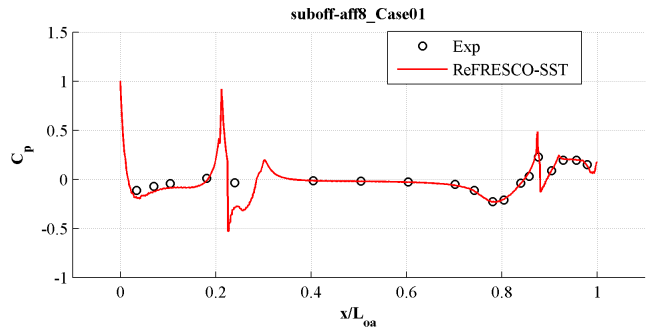


Figure 16. Pressure coefficient along the hull, $\beta = 0^\circ$

Table 11. Longitudinal force X , AFF-8, $Re = 1.2 \times 10^7$, $\beta = 0^\circ$

Solver	Grid	Integral values $\times 10^3$			
		X	X_f	X_p	ϵ_X (%)
ITTC-57		-	-1.015	-	-
Schoenherr		-	-0.995	-	-
Katsui		-	-0.980	-	-
Grigson		-	-1.004	-	-
ReFRESCO-SST	4866×10^3	-1.257	-1.040	-0.217	-
(AFF-1)	4138×10^3	-1.126	-0.993	-0.113	-

Flow Analysis

Straight flight, $\beta = 0^\circ$ Comparing the forces and moments for AFF-8 and AFF-1 presented in Table 10 one can see that the drag force X has increased more than 11%, and that the submarine even for straight flight is subjected to a vertical force Z (downwards) and a bow-up pitching moment M . This means that the submarine will tend to pitch in a bow-up attitude, just due to the appendages, which must be compensated using ballast or by adjusting the diving planes. Table 11 shows a more detailed comparison of the longitudinal force for AFF-8 and AFF-1. The wetted area of AFF-8 is about 5.7% larger than the wetted area of AFF-1, which results in a larger friction resistance: for AFF-8, X_f increased in magnitude by about 4.7%. The remainder of the increase of the resistance is due to an increase of the form factor: $(1+k) = X/X_f = 1.21$ for AFF-8 and $(1+k) = 1.13$ for AFF-1.

The form factor for the AFF-8 is judged to be slightly higher than average for appended submarines.

The flow is smooth with respect with the hull and appendages, and does not present considerable flow separation, not even close to any of the protruding appendages. The sail or bridge fairwater presents a pressure distribution characteristic of a symmetric wing, with lower pressure distributions close to the leading-edge. The wake of the wing is just due to the viscous boundary layer velocity deficit (no lift) and extends down to the propeller disk. Close to the junction of the sail with the hull, and stern-appendages with the hull, so-called *horse-shoe* vortices arise, see Figure 18. These are caused by the displacement of the boundary layer of the hull when it feels the adverse pressure gradient close to the stagnation point of the sail and wings. All these effects can be captured by steady RANS calculations on a fine grid and are reflected in the wake shown in Figure 17.

Oblique flight, $\beta = 18^\circ$ A computation for an inflow angle of $\beta = 18^\circ$ has been also done for the AFF-8 configuration.

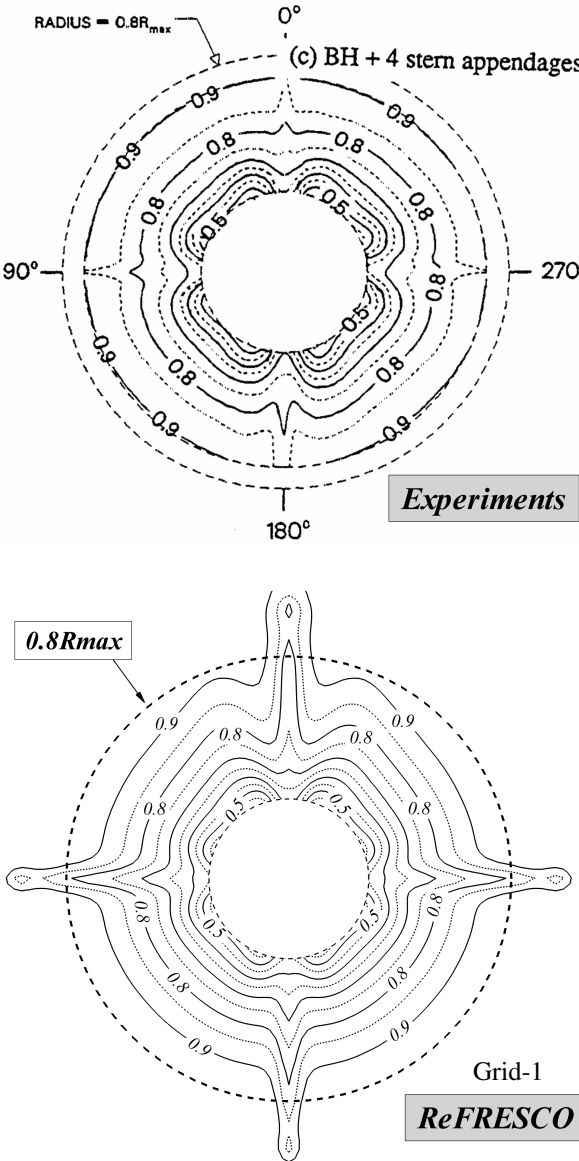


Figure 17. Wake-field V_x/V_0 at $x/L_{\text{oa}} = 0.978$, $\beta = 0^\circ$

Table 12. Forces and moments, AFF-8, $Re = 1.2 \times 10^7$, $\beta = 18^\circ$

Solver	Grid	Integral values $\times 10^3$			
		X	X_f	X_p	ϵ_X (%)
ReFRESCO-SST	2382×10^3	-0.850	-1.083	0.233	-
ReFRESCO-SST	2382×10^3	Y	Y_f	Y_p	ϵ_Y (%)
ReFRESCO-SST	2382×10^3	Z	Z_f	Z_p	ϵ_Z (%)
ReFRESCO-SST	2382×10^3	K	K_f	K_p	ϵ_K (%)
ReFRESCO-SST	2382×10^3	0.116	-0.002	0.119	-
ReFRESCO-SST	2382×10^3	M	M_f	M_p	ϵ_M (%)
ReFRESCO-SST	2382×10^3	0.611	0.006	0.605	-
ReFRESCO-SST	2382×10^3	N	N_f	N_p	ϵ_N (%)
ReFRESCO-SST	2382×10^3	2.973	0.014	2.958	-
ReFRESCO-SST	2382×10^3	(M/Z)	$(M/Z)_f$	$(M/Z)_p$	$\epsilon_{(M/Z)}$ (%)
ReFRESCO-SST	2382×10^3	0.097	1.234	0.096	-
ReFRESCO-SST	2382×10^3	(N/Y)	$(N/Y)_f$	$(N/Y)_p$	$\epsilon_{(N/Y)}$ (%)
ReFRESCO-SST	2382×10^3	0.251	0.053	0.255	-

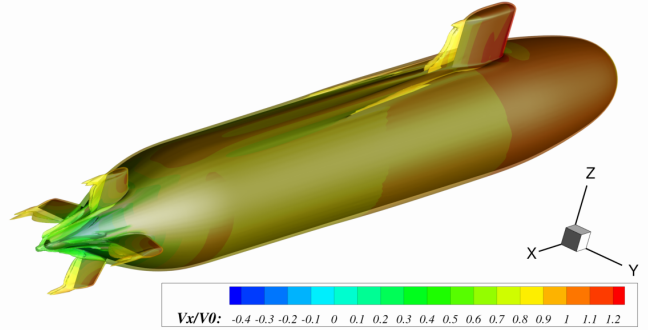


Figure 18. Total non-dimensional vorticity $\omega L_{\text{pp}}/V_0$ iso-surface=50 coloured with V_x/V_0 contours for AFF-8, $\beta = 0^\circ$, Grid-1

Due to the existence of the sail, which has a considerable thickness, and the large inflow angle, one can expect that the flow will separate in the suction side of this appendage. Large separation areas are not stable, induce vortex shedding and therefore lead to unsteady flow. The computations were done in steady mode but the forces and moments iterative history shows some modulation. This means that the computations should be done in unsteady mode. This will be further investigated in the future.

The forces and moments on the hull are presented in Table 12. Compared to the AFF-1 results (for $Re = 14 \times 10^{-6}$), an increase in transverse force Y is seen as expected, due to the lift generated by the sail and stern rudders. Furthermore, the yawing moment N slightly reduces, due to the stabilising effect of the stern rudders. The shift in the de-stabilising arm N/Y is considerable, i.e. $N/Y = 0.63$ for AFF-1 and 0.25 for AFF-8. Due to the drift angle, large out-of-plane forces and moments are generated as expected. This is caused by the carry-over of the bound vortex on the sail to the hull. This bound vortex in combination with the cross flow results in a downward force distribution aft of the sail and subsequently a downward Z force and positive pitch moment M.

Figure 19 shows the axial velocity contours for several transverse planes along the sail of the submarine. There is a large separated area at the leeward side of the sail. The vortices shed there are pulled down into the low pressure area at the leeward side of the hull and enter the propeller plane. Also, the sail has lift and therefore its wake is stronger and a tip-vortex is generated. This vorticity is also sucked to the hull and into the propeller disk.

At port side of the submarine the flow is smooth and follows

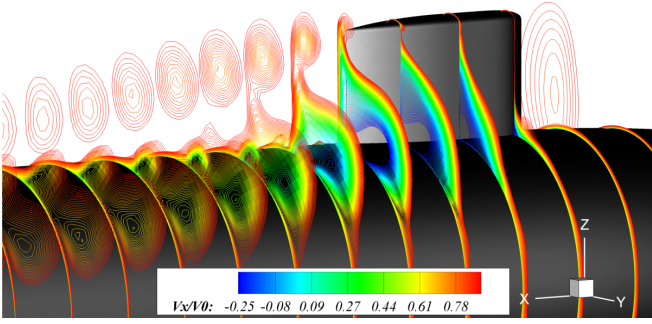


Figure 19. V_x/V_0 contours for AFF-8, $\beta = 18^\circ$, Grid-4

the circular hull. At starboard Von Karman vortices typical of blunt-body flows are formed. These are disturbed by the previously referred features, but in the bottom of the hull they remain visible (see Figure 21). These will also induce unsteady flow. The wake field of the submarine is therefore highly asymmetrical and contains several vortical structures, as shown in Figure 20. When a propeller is operating in this wake field its performance will deteriorate and cavitation can occur at lower depths. Nevertheless, with an operating propeller the wake-field is also different than without operating propeller. This will be considered in a future phase.

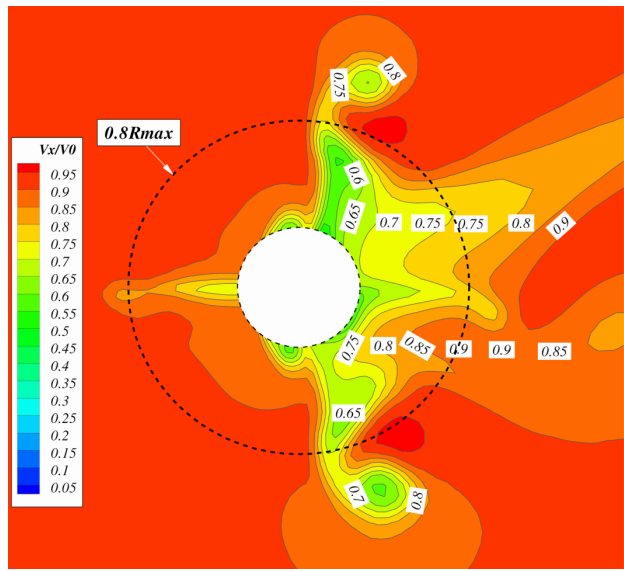


Figure 20. Wake-field V_x/V_0 at $x/L_{\text{oa}} = 0.978$, $\beta = 18^\circ$, Grid-4

Comparisons We now compare and analyse the flow fields for both configurations and for $\beta = 0$ and 18° . Figure 21 shows the total non-dimensional vorticity contours for AFF-1 at 0° , AFF-8 at 0° , AFF-1 at 18° and AFF-8 at 18° . For the AFF-1 case, the results on the half domain have been mirrored for the visualisation. The small vortical structures for $\beta = 0^\circ$ close to the symmetry line are not physical but due to this mirroring. For the rest of the hull, the flow is aligned with the surface and the only vorticity visible is due to the boundary layers (transversal and not axial vorticity). For AFF-8 and the same angle of attack, the major flow features have already been explained, but it is interesting to see that the sail wake goes into the propeller disk and that horse-shoe vortices are visible close to the sail and stern appendages.

For the AFF-1 at 18° , long and stretched Von Karman vortex

shedding patterns typical of blunt-body flows are visible. The computations have been done also using a symmetry plane at half of submarine. From this vorticity field, one can say that this is not the most correct choice since this will inhibit the unsteady shedding of the vortices and therefore also might change the forces on the submarine. As already referred, for this test case, one can expect that a RANS approach will lead to worse results than a DES/DDES or LES approach [22]. For the AFF-8 at 18° , the complete submarine has been simulated and thus no symmetry plane used. The effect of it is an unsteady modulation in the resulting forces. Here, the sail and the stern appendages dominate the flow more than the smooth port side bare hull. One could expect that for this geometry better results would be obtained by RANS than for the bare hull.

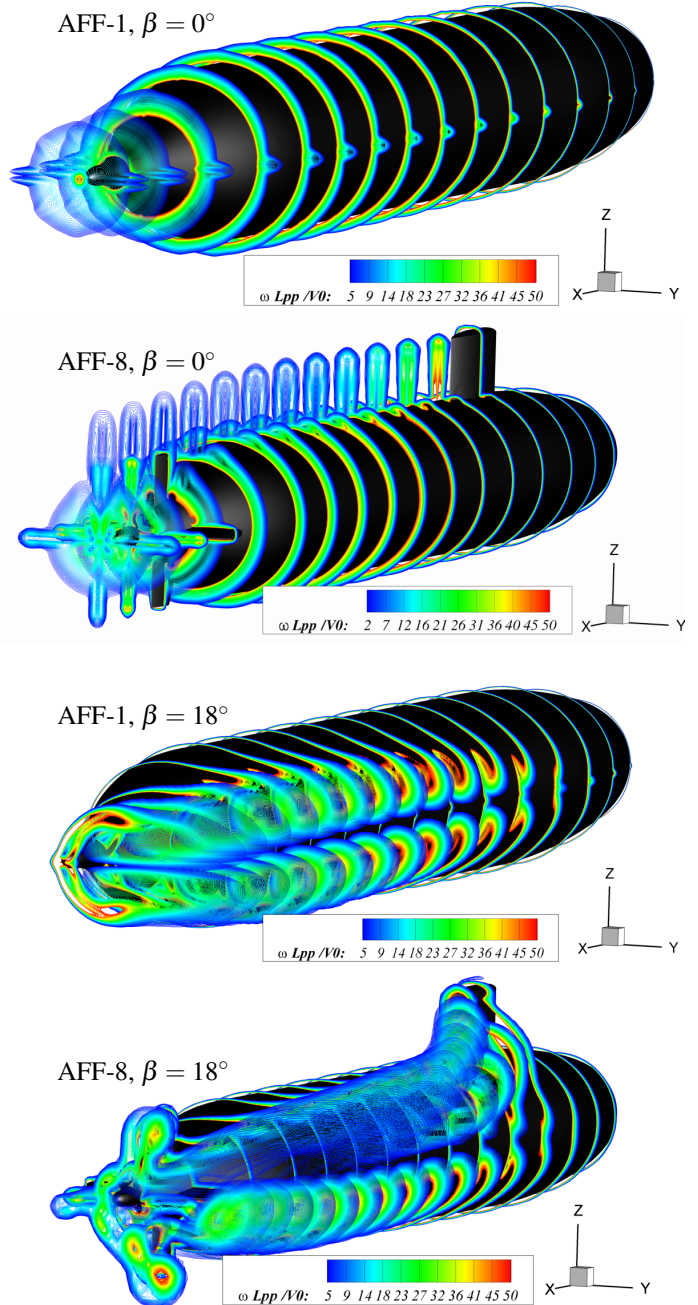


Figure 21. Total non-dimensional vorticity $\omega L_{\text{pp}}/V_0$ contours

Forced Pitch Motion Simulation

In this last example, we use *AcuSolve* to calculate the pitching moment on the AFF-8 configuration undergoing a forced pitching motion, and we compare this moment with a simple static analysis. In this simulation, the submarine is moving horizontally when it undergoes a sinusoidal forced pitch motion from 0° to 10° and back to 0° in which the pitch angle θ is defined by,

$$\theta = 5^\circ + 5^\circ \sin\left(-\frac{\pi}{2} + \frac{2\pi t^*}{T}\right), \quad (1)$$

when $0 < t^* < T$, with $t^* = tV_0/L_{oa}$ and $T = 5.0$ is the chosen period for the manoeuvre. For the static approach the submarine is set to a pitch angle of 10° and the moment computed using *AcuSolve* after all numerical transients have decayed. With this moment, a linear formula $M = M_\theta \cdot \theta$ is considered, from which the constant M_θ is computed. For the pitching motion explained above, this linear formula is then used to compute the moments. For the dynamic approach the pitching manoeuvre is simulated using an unsteady computation with the submarine pitch angle varying in time according to Equation 1. Figure 22 shows the results of both approaches. The acceleration is large in the beginning and at the end of the manoeuvre. Here the added-mass is important, and this effect is missed in the static approach. As known, this added-mass effect induces a phase change between the maximum angle and the maximum moment but also the amplitude of the moment. This effect is not negligible.

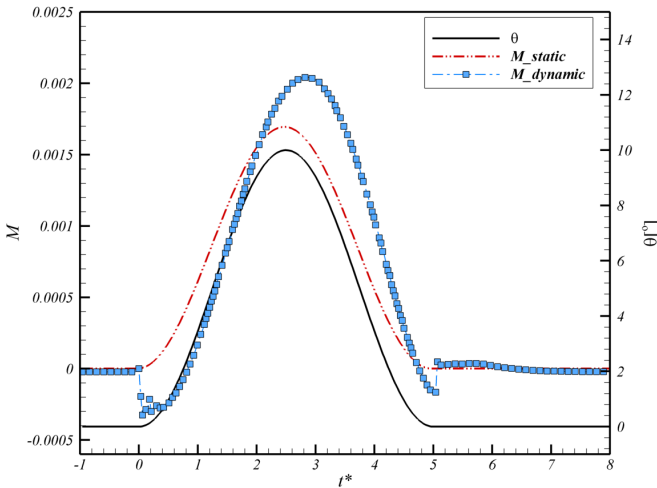


Figure 22. Comparison of CFD static and dynamic approach

CONCLUSIONS

Calculations on the bare and appended DARPA SUBOFF hull-form sailing straight ahead and at oblique motion were conducted in order to verify the accuracy of the predictions using two viscous-flow solvers: MARIN in-house code *ReFRESCO* and commercial code *AcuSolve*. Based on this study, it is concluded that both solvers are capable of predicting the flow around a submarine hull form. Comparisons of the predictions with experiments give good agreement. It has been also seen that dynamic manoeuvre simulations are possible with CFD codes.

Using a steady RANS approach, detailed verification studies using nine grids have been performed and validation with experimental data for both integral and local quantities was done. For a DDES approach this was not done since grid-independence is

not a trivial task: the more grid nodes, the more scales are simulated and less are modelled and therefore the results will change. This is a topic under discussion within the CFD community. The DDES unsteady results by *AcuSolve* present better agreement with the experiments for larger angles than the RANS steady results by *ReFRESCO*. This is understandable based on the flow field visualisations here presented and the well known problems with RANS for simulating large shear-layer areas. For the appended configuration we expect however the RANS results to be more accurate than for the bare hull due to the geometry complexity which defines the flow, which is completely captured. In fact, *ReFRESCO* results for the appended hull, for straight-flight, presented a good agreement with the experimental data available. The results also showed the complexity of the flow field for oblique-flight, which is a combination of a blunt-body type of flow around the cylindrical hull, flow around lifting appendages, and interaction between both. The wake-fields at the propeller location are rich in vortical structures and very different from typical ship wake-fields.

Based on the results here presented we will consider in the short-future the following additional studies:

- Perform verification studies for the AFF-8 appended hull.
- Perform unsteady computations using RANS for angles above 18° , both for the bare and appended hulls.
- Implement DDES in *ReFRESCO* which is not a very difficult task, but deserves extra careful validation, and compare the results with the *AcuSolve* results.
- Perform more dynamic manoeuvres with both codes and compare the results.

ACKNOWLEDGEMENTS

Part of the work presented here was funded through TNO Defence, Security and Safety within the framework of Programma V705 carried out for DMO of the Royal Netherlands Navy. Their support is greatly acknowledged. Thanks also to Christiaan Klaij from MARIN for making the *GridPro* grids for the AFF-8 configuration.

REFERENCES

- [1] Sung, C.-H., Griffin, M., Tsai, J., and Huang, T., 1993. "Incompressible flow computation of forces and moments on bodies of revolution at incidence". *31st Aerospace Sciences Meeting and Exhibit, AIAA-1993-787*, January.
- [2] Huuva, T., 2008. "Large Eddy Simulation of Cavitating and Non-cavitating flow". PhD thesis, Chalmers University of Technology, February.
- [3] Toxopeus, S., and Vaz, G., 2009. "Calculation of Current or Manoeuvring Forces using a Viscous-Flow Solver". *In Proceedings of OMAE2009, Honolulu, Hawaii, USA*, June.
- [4] Groves, N., Huang, T., and Chang, M., 1998. "Geometric characteristics of DARPA SUBOFF models (DTRC Model Nos. 5470 and 5471)". *Report No. DTRC/SHD-1298-01*, March.
- [5] Huang, T., Liu, H.-L., Groves, N., Forlini, T., Blanton, J., and Gowing, S., 1992. "Measurements of flows over an axisymmetric body with various appendages in a wind tunnel: the DARPA SUBOFF experimental program". *19th Symposium on Naval Hydrodynamics*, August, pp. 312–346.
- [6] Liu, H.-L., and Huang, T., 1998. "Summary of DARPA SUBOFF experimental program data". *Report No. CRDKNSWC/HD-1298-11*, June.
- [7] Bull, P., 1996. "The validation of CFD predictions of nominal

- wake for the SUBOFF fully appended geometry". *21st Symposium on Naval Hydrodynamics*, June, pp. 1061–1076.
- [8] Yang, C., and Löhner, R., 2003. "Prediction of flows over an axisymmetric body with appendages". *8th International Conference on Numerical Ship Hydrodynamics*, September.
- [9] Alin, N., Fureby, C., and Svennberg, S., 2003. "LES of the Flow past Simplified Submarine Hulls". *In the Proceedings of 8th International Conference on Numerical Ship Hydrodynamics, Busan, Korea*.
- [10] Roddy, R., 1990. "Investigation of the stability and control characteristics of several configurations of the DARPA SUBOFF model (DTRC Model 5470) from captive-model experiments". *Report No. DTRC/SHD-1298-08*, September.
- [11] Vaz, G., Jaouen, F., and Hoekstra, M., 2009. "Free-Surface Viscous Flow Computations. Validation of URANS Code FRESCO". *In Proceedings of OMAE2009, Honolulu, Hawaii, USA*, June.
- [12] Vaz, G., Waals, O., Fathi, F., Ottens, H., Le Souef, T., and Kwong, K., 2009. "Current Affairs - Model Tests, Semi-Empirical Predictions and CFD Computations for Current Coefficients of Semi-Submersibles". *In Proceedings of OMAE2009, Honolulu, Hawaii, USA*, June.
- [13] Fathi, F., Klaij, C., and Koop, A., 2010. "Predicting Loads on a LNG Carrier with CFD". *In Proceedings of OMAE2010, Shanghai, China*, June.
- [14] Koop, A., Klaij, C., and Vaz, G., 2010. "Predicting Wind Shielding for FPSO Tandem Offloading using CFD". *In Proceedings of OMAE2010, Shanghai, China*, June.
- [15] Hughes, T., Franca, L., and Hulbert, G., 1989. "A New Finite Element Formulation for Computational Fluid Dynamics. VII. The Galerkin/least-squares Method for Advective-Diffusive Equations". *Computational Methods in Applied Mechanics*, **73**, pp. 173–189.
- [16] Shakib, F., Hughes, T., and Johan, Z., 1991. "A New Finite Element Formulation for Computational Fluid Dynamics. X. The compressible Euler and Navier-Stokes Equations". *Computational Methods in Applied Mechanics*, **89**, pp. 141–219.
- [17] Jansen, K. E., Whiting, C. H., and Hulbert, G. M., 2000. "A Generalized-Alpha Method for Integrating the Filtered Navier-Stokes Equations with a Stabilized Finite Element Method". *Computational Methods in Applied Mechanics*, **190**, pp. 305–319.
- [18] Constantinides, Y., Oakley, O., and Holmes, S., 2007. "CFD High L/D Riser Modeling Study". *In Proceedings of OMAE2007, Estoril, Portugal*.
- [19] Holmes, S., 2008. "Predicting Spar VIM using CFD". *In Proceedings of OMAE2009, Honolulu, Hawaii, USA*.
- [20] Spalart, P., and Allmaras, S., 1992. "A One-Equation Turbulence Model for Aerodynamic Flows". *In the Proceedings of AIAA 30th Aerospace Sciences Meeting, Reno, Nevada, USA*(AIAA Paper 92-0439).
- [21] Menter, F., 1994. "Two-equation Eddy Viscosity Turbulence Models for Engineering Applications". *AIAA Journal*, **32**, pp. 1598–1605.
- [22] Spalart, P., Deck, S., Shur, M., Squires, K., Squires, M. K., and Travin, A., 2005. "A New Version of Detached Eddy Simulation, Resistant to Ambiguous Grid Densities". *Theoretical and Computational Fluid Dynamics*.
- [23] Eça, L., and Hoekstra, M., 2005. "On the influence of grid topology on the accuracy of ship viscous flow calculations". *5th Osaka Colloquium on Advanced CFD Applications to Ship Flow and Hull Form Design*, March, pp. 1–10.
- [24] Vaz, G., Mabilat, C., van der Wal, R., and Gallagher, P., 2007. "Viscous Flow Computations on Smooth Cylinders. A Detailed Numerical Study with Validation". *In Proceedings of OMAE2007, San Diego, California, USA*, June.